Acta Astronautica 238 (2026) 744–754

Contents lists available at ScienceDirect

Acta Astronautica

journal homepage: www.elsevier.com/locate/actaastro

Research paper

Investigating the impact of different ion species and materials on Electrodynamic Tether current collection efficiency ☆

Shagun Aggarwal [a,b,d,*], Josef Richmond [c], Andrew Dempster [a,b], Jason Held [b,d], Rod Boswell [c]

[a] Australian Center for Space Engineering Research (ACSER), UNSW, Sydney, NSW, Australia
[b] The ARC Industrial Transformation Training Center for CubeSats, UAVs, and Their Applications (CUAVA), Australia
[c] Space Plasma, Power and Propulsion Laboratory (SP3), Australian National University, Canberra, ACT, Australia
[d] Saber Astronautics, 95 Rose Street, Chippendale, Sydney, 2008, NSW, Australia

ARTICLE INFO

Keywords:
Electrodynamic Tether
Orbital motion limited
Plasma experiment
Ion species effects

ABSTRACT

This paper describes the analysis and comparison of the electron current collection of a cylindrical tether for different variables like plasma density and temperature, plasma ion species, tether material, and applied bias. The plasma is generated by ionizing hydrogen, oxygen, and ambient air in a 50 cm × 40 cm plasma chamber. Multiple plasma densities were generated in the range 10^{14}–10^{15} particles per m^3 with corresponding plasma temperatures 2.5–4.3 eV. EDT materials — aluminum, tungsten, and aracon were used in the experiment to examine the material performance in the generated plasma environment and evaluate the impact on the current collected. Several observations have been made from the data collected. The I-V curves vary due to each ionized plasma, indicating the impact of ion species on the electron current. The OML model overestimates the current for each experiment run analyzed. Aracon sample exhibited superior performance when placed in oxygen and air plasma, whereas aluminium demonstrated higher I-V curves in hydrogen plasma. Plasma bubbles and secondary plasma were observed during the experiment for both positively and negatively biased tether samples. In the positively biased regime, anomalous electron current occurred for certain plasma densities. In the negatively biased regime, the ion current for hydrogen plasma was recorded to be higher than the oxygen and air plasma. It was concluded that the OML does not accurately estimate the collected current, as more complex interactions are involved.

1. Introduction

An Electrodynamic Tether (EDT) is a space-borne conducting wire that generates a Lorentz force when interacting with Earth's magnetic field. Motion of the tether in the conducting plasma creates an electromotive force causing the electric potential induced to go from highly positive potential to highly negative between the two ends of the tether. As a result, a current flows through the tether length, inducing a Lorentz force. The Lorentz force generated can provide propellantless propulsion for applications such as deorbiting, power generation, orbit maneuvering, and station keeping. The efficiency of an EDT system depends on the electrical connection between the plasma and tether for current collection.

Tethered satellite system - 1 (TSS-1) and TSS-1R missions used a conducting spherical end body as a plasma contactor for electron collection [1,2]. The plasma motor generator experiment (PMG) used a 500 m insulated tether with hollow cathodes for electron collection and emission [3]. Later, leaving a section of the tether or its entire length bare was suggested as an alternative to end-body plasma contactors for electron collection. NASA's Propulsive Small Expendable Deployer System (ProSEDS) was the first mission designed to test the bare tether concept. The mission was eventually canceled but since then many missions have adopted the bare tether approach [4].

When a tether is left bare, biased by the induced potential difference or an external power source it collects an electron current at

☆ This work presents the experimental investigation of EDT current collection efficiency under different ion species and tether material conditions in a laboratory plasma environment. The study compares aluminum, tungsten, and aracon samples in hydrogen, oxygen, and air plasmas, highlighting deviations from OML theory due to neutral particle effects and secondary plasma formation.

* Corresponding author at: Australian Center for Space Engineering Research (ACSER), UNSW, Sydney, NSW, Australia.
E-mail addresses: shagun.aggarwal@unsw.edu.au (S. Aggarwal), Josef.Richmond@anu.edu.au (J. Richmond), a.dempster@unsw.edu.au (A. Dempster), jheld@saberastro.com (J. Held).

https://doi.org/10.1016/j.actaastro.2025.10.030
Received 14 July 2025; Received in revised form 10 September 2025; Accepted 15 October 2025
Available online 21 October 2025

the positive end and a low ionic at the negative end from ambient plasma [5]. For a given bias potential, plasma probe theory predicts that the collected electron current per unit area is maximized in the orbital-motion-limited (OML) regime for thin cylindrical wires. For a thin cylindrical probe to operate in the OML regime, the radius of the probe (r) should be smaller than the Debye length (λ_D) and the electron gyroradius. The Debye Length is a function of the electron density and the gyro radius is the radius of the circular motion of charged particles in the presence of a magnetic field. The OML regime ensures effective sheath formation resulting in the highest current collection efficiency. The theoretical two-dimensional OML current is given as follows:

$$I = N_e A_p \frac{\sqrt{2}}{\pi} v_{te} \sqrt{1 + \frac{q\Delta V}{kT_e}} \tag{1}$$

where,

N_e = Electron Density (particles per m^{-3}), T_e = Plasma Temperature, A_p = Probe Area, m_e = electron mass, q = Electron charge, k = Boltzmann Constant, ΔV = Applied Potential - Plasma potential, v_{te} (Thermal Velocity) = $\sqrt{\frac{kT_e}{m_e}}$

For high potentials ($\Delta V \gg \frac{kT_e}{m_e}$), Eq. (1) reduces to

$$I_{thermal} = N_e A_p \frac{\sqrt{2}}{\pi} \sqrt{\frac{q\Delta V}{kT_e}} \tag{2}$$

When the bare tether operates in the OML regime, the current collected is the upper limit to the current that can be collected by the round cylindrical probe in a collision-less plasma, quasi-static, uniform, non-flowing, unmagnetized maxwellian plasma. Although the OML method of modeling the current induced in a tether is widely accepted, a high degree of simplification is required to derive the OML theory. Due to this several precautions are taken to ensure that the EDT is designed to operate in the OML regime for current collection. While such simplifications do not reflect the complex plasma environment in LEO accurately, a question arises of how variables of such a complicated system impact the current collection of an EDT. There is a need to understand the influence of different variables on the current collected in a bare tether.

The aim of this experiment is to evaluate the impact of multiple variables on tether current collection. I-V curves of the tether sample of materials — aluminum, aracon, and tungsten are evaluated for plasma simulation. Hydrogen, oxygen, and room air are ionized in a plasma chamber setup to simulate LEO condition at different altitudes. The impact of dominant ion species on the electron current is examined for tether samples. In this study, the OML model is used as a baseline when comparing the I-V curve data when changing different variables.

2. Experimental setup

2.1. Plasma chamber setup

The plasma chamber experiments were conducted at the plasma chamber of the SP3 (Space Plasma, Power and Propulsion) group facility located at the Australian National University (ANU) in Canberra [6]. The chamber dimensions are 50 cm by 40 cm in length and width. The plasma chamber has a mount that holds the tether sample, and the sample is connected to the base of the chamber to maintain the straight length of the sample. The top of the chamber is connected to the pressure gauge that tells us what the pressure in the chamber is. The plasma is generated in a glass tube. The glass tube is where the plasma is generated and is connected to the gas feed. The gas is provided from the gas cylinder which is connected to the gas feed as it can be seen in Fig. 1. The plasma source is connected to the matching box which matches the impedance of the plasma to the plasma generator so that no power is reflected to the generator and all plasma goes to the generator. The matching box is connected to the SWR meter which measures the power that goes into the impedance matchbox, to see how power forwards us and how much is reflected.

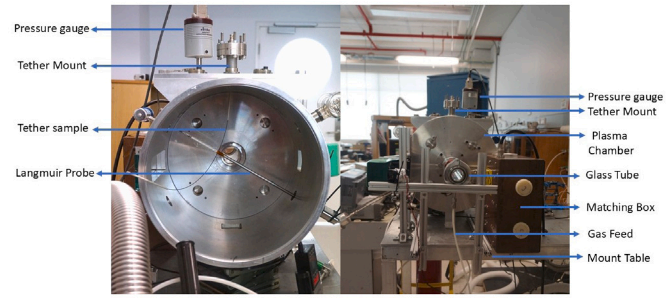

Fig. 1. The plasma chamber setup at the ANU SP3 Laboratory. Left: Internal view of the plasma chamber setup with a tether sample mounted on the chamber ceiling and a Langmuir probe placed perpendicular to incoming plasma, Right: External view of the plasma chamber with connected glass tube and matchbox capacitor.

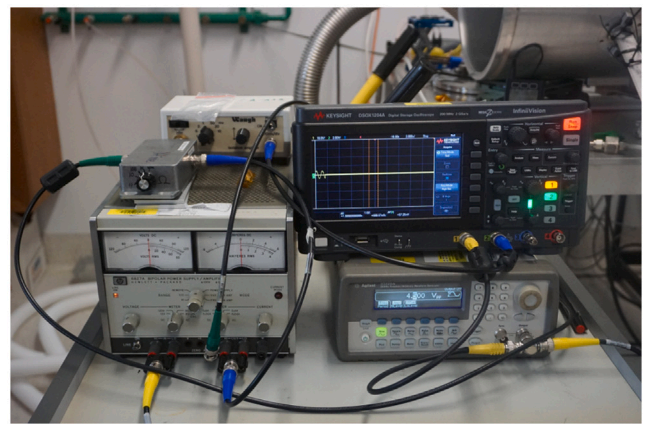

Fig. 2. Data Measurement Setup.

The pressure of the gas flow in the chamber is maintained by the following circuit. There is a pressure gauge reader is the pressure which gives the reading from the pressure gauge. The cooling fan power source is a part of this circuit that controls the fan for cooling the glass tube so that it does not get too heated. The plasma generator has settings that consist of the base power (on/off), RF power (on/off), and Power dial for increasing/decreasing the power for the plasma generation. The flip side of the plasma chamber is where the tether setup can be seen. There is a window through which we can see the tether. The tether mount which is outside the plasma chamber wall has a base attachment that places the sample in the chamber and Langmuir probe.

2.2. Data collection and measurement

Fig. 2 describes the electrical setup for the electron current data collection. The setup includes the following equipments :

1. Resistor box
2. Function generator
3. Bi-polar amplifier fixed gain (−20 V approx. 18.5 V)
4. Oscilloscope
5. Function generator — This is where we are using to generate a sine wave which generator 10 Vpp voltage sweeps as we want to get data for tether positively and negatively biased tether.
6. Langmuir Probe — The LP is an RF compensated probe meaning it is a system that attenuates an RF signal so that there is no RF signal would create noise in the readings.

Table 1
Characteristics of tether samples used in the experiment.

Tether sample	Material	Radius	Resistivity (Ωm)	Conductivity (σ)	Melting Point (°C)
Sample 1	Tungsten	0.7 mm	52.8×10^{-8}	1.79×10^{7}	1453
Sample 2	Aluminium	0.9 mm	2.65 to 2.82×10^{-8}	3.5×10^{7}	660
Sample 3	DragEN Tether	0.5 mm	6.99×10^{-8}	1.43×10^{7}	1453

2.3. Tether sample

Three different sample materials have been taken for use during these tests: Aluminium, Tungsten, DragEN Tether. Tungsten has been the preferred sample in previous investigations because it can endure high temperatures caused by a collection of high-energy electrons [7–9]. Aluminium is a widely available material often used in space missions for a magnitude of applications. Samples of bare tether consist of an aluminum core and synthetic fiber to reinforce the tether, either twisted or braided. Some other samples of the bare tether samples considered are CT-104, CT-207, and ARACON (aluminum core and synthetic fibers) [10]. Thus, the final sample considered is the DragEN Tether by Saber Astronautics made of ARACON. Aracon is a family of metal-clad fibers that has the conductivity of metal with the strength, lightweight, and flexibility of Kevlar fibers. These fibers provide a versatile combination of physical and electrical properties for a variety of demanding applications. The DragEN tether is coated with nickel to offer superior thermal stability, while still being 60% lighter than copper wire [11].

The length of each sample is approximately 30 cm and are attached at the top and bottom of the chamber wall. The samples are placed perpendicular to the flow of the plasma. Fig. 1 shows the interior view of the plasma chamber with the tether attached to the ceiling and bottom of the chamber. Table 1 shows the characteristics of the tether samples taken.

2.4. Plasma simulated

Different gases have been used to simulate plasma in LEO at varying altitudes. The ionosphere is divided into different altitude ranges, with O_2^+ and NO^+ being the main ion species below 500 Km altitude. Above 600 Km altitude, the predominant ion species are H^+ and He^+. At higher altitudes, the concentration of H^+ is greater than that of He^+. Three plasma sources were utilized in this experiment to replicate the LEO environment. The objective was to investigate the effects of various radiation environments on different ion species within the plasma chamber. This was done to imitate the plasma composition found at different altitudes. The following gases were used to simulate the plasma in the experiment are as follows:

1. Hydrogen
2. Oxygen
3. Air

A 13.56 MHz RF was used to generate plasma using hydrogen, oxygen and air in the glass tube, and allowed to diffuse into the primary chamber. Changing the pressure in the plasma chamber results in variations in the plasma density. The plasma simulated is assumed to be quasi-neutral i.e. $n_e = n_i$. Multiple experiment runs (scopes) of time series data were recorded with varying different densities and gaseous sources as parameters. The tether sample was biased with a linear staircase I-V sweeps from −80 V to +80 V. To assess the influence of tether biasing on the current obtained, the samples were additionally biased within the range of −120 V to +120 V, for scopes where minimal activity was observed. All the probe samples were biased with respect to the plasma chamber. The Plasma is generated using the following two methods [12]:

1. Inductive plasma: Inductive plasma is generated by passing a high-frequency electrical current through a coil of wire, creating a magnetic field that ionizes the gas within the coil. As the electrons of the gas particles are freed up, the gas becomes electrically conductive. This allows an even higher energy deposition into the gas.

2. Capacitive plasma: is mostly on E field, works like a capacitor and generating field to ionize the gas (AC $E^{\rightarrow}$ field). In this configuration, the RF power is applied to an electrode, often a metal plate or coil, which is separated from the plasma by a dielectric material. The capacitance created between the electrode and the plasma allows for efficient transfer of RF energy to the gas, leading to ionization and the formation of a plasma.

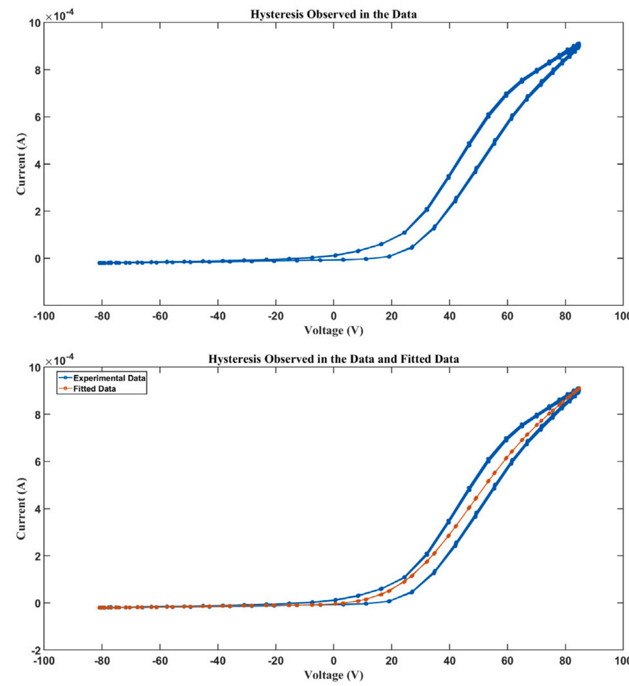

Fig. 3. Hysteresis observed in the raw data collected from the plasma chamber experiment and the curve resulting from smooth spline fitting applied to the data.

For all the densities that have been simulated to study the influence of the variation radiation environment. Since many densities were simulated, the main idea was to compare it with OML conditions to compare with the OML conditions of the radius of the tether. This is important as the OML conditions should be met, with the current parameters the OML condition is met in every condition. The range of densities generated for all the plasma gases are shown in Tables 2, 3 and 4.

3. Data hysteresis

When the I-V data are plotted, hysteresis is observed in the data as seen in Fig. 3. The scope plotted here shows the voltage sweep from −80 V to +80 V for reference in Fig. 3. The hysteresis visible in the I-V curves arises from these voltage sweeps, with the difference in current collection between the forward and reverse sweeps creating the observed loop. To address this issue, the data was smoothed using spline fitting, which effectively reduced the hysteresis and produced the results as shown in Fig. 3.

Table 2
Hydrogen gas plasma densities simulated.

Pressure (mTorr)	Power (W)	Mode	Temperature (eV)	Density (particles m^{-3})
100	120	Inductive	2.57	6.67×10^{14}
80	120	Inductive	2.84	7.06×10^{14}
60	120	Inductive	3.46	8.23×10^{14}
40	120	Inductive	3.59	9.23×10^{14}
20	120	Inductive	3.74	1.21×10^{15}
17	120	Inductive	3.85	1.02×10^{15}
15	120	Inductive	3.91	1.11×10^{15}
13	120	Inductive	4.01	1.13×10^{15}
20	80	Capacitive	3.67	3.53×10^{14}
17	80	Capacitive	3.96	3.90×10^{14}
15	80	Capacitive	4	5.10×10^{14}
13	80	Capacitive	4.1	7.32×10^{14}
10	80	Capacitive	4.21	8.53×10^{14}
5	80	Capacitive	4.30	9.68×10^{14}
1	80	Capacitive	3.51	3.08×10^{14}

Table 3
Oxygen plasma densities simulated.

Pressure (mTorr)	Power (W)	Mode	Temperature (eV)	Density (particles m^{-3})
40	120	Inductive	3.42	1.32×10^{14}
20	120	Inductive	3.34	7.30×10^{14}
17	120	Inductive	3.65	8.58×10^{14}
15	120	Inductive	3.65	5.70×10^{14}
13	120	Inductive	3.673	6.01×10^{14}
10	120	Inductive	3.68	6.30×10^{14}

Table 4
Air plasma densities simulated.

Pressure (mTorr)	Power (W)	Mode	Temperature (eV)	Density (particles m^{-3})
40	120	Inductive	3.24	3.00×10^{14}
20	120	Inductive	3.37	4.30×10^{14}
17	120	Inductive	3.48	5.40×10^{14}
15	120	Inductive	3.50	5.67×10^{14}
13	120	Inductive	3.63	7.73×10^{14}
10	120	Inductive	3.71	8.68×10^{14}

This approach helped mitigate the effects of hysteresis while preserving the overall trends in current collection, allowing for a more accurate analysis of tether performance across different voltage biases. Due to the volume of data points collected in each scope, the addition of error bars complicates data representation; hence, error bars have not been incorporated into the I-V plots.

4. Current collection data

All the densities for the experiment runs (scopes) are plotted in the Figs. 4, 5, 6 and 7. The data plots present the current as a function of voltage showcasing the data recorded for each tether sample considered (aluminum, DragEN Tether, tungsten) for each radiation (hydrogen, oxygen and air) as indicated in Tables 2, 3 and 4.

The bias was applied to the tether samples in sweeps of the ranges -80 V to 80 V to observe the I-V curve profiles in the positively biased and negatively biased tether. These values are significantly higher than the densities observed in the LEO environment. Within the LEO environment, the plasma density normally falls within the range of 10^{11} to 10^{12} particles per cubic meter and the plasma temperature varies between 0.1 eV and 0.2 eV. The plots include calculated OML values using Eqs. (1) and (2) alongside the experimental data. As per the OML model EDT's radius must be shorter than the debye length and the plasma's electron gyroradius when operating in the OML domain to avoid the effects of space charge shielding and magnetic guiding. The densities generated in the experiment, the debye length exceeds the radius of all tether samples. Previous investigations have shown that the loss in performance of the tether sample collected occurred gradually [7].

5. Impact of plasma composition

EDTs rely on the interaction between the tether and surrounding plasma to generate electrical currents. The conductivity of the plasma directly impact the power generation and propulsion functionalities. Investigating various plasma compositions is essential to identify the impact of dominant ions on EDT performance and use it to enhance EDT systems' effectiveness. In this experimental investigation, different densities of plasma are produced at different operating pressures by ionizing air, hydrogen gas, and oxygen gas. Figs. 4, 5, 6 and 7 show all I-V characteristics graphs for all the densities simulated for air, hydrogen, and oxygen plasma respectively. The experimental data and the computed OML values are plotted, compared, and analyzed.

5.1. Hydrogen plasma

In this section the I-V curves for the tether samples in hydrogen plasma are plotted and discussed in Figs. 4 and 5. The particle number densities generated are in the range from 10^{14}–10^{15} particles m^{-3}. The hydrogen plasma was generated using inductive and capacitive methods with a aim of generating lowest possible densities. Hydrogen ions (H^+) have a low ionic mass of 1 amu, resulting in a higher ion sound speed. Compared to heavier ions such as O^+, lighter H^+ ions exhibit greater mobility, leading to potentially higher ion currents in hydrogen plasma compared to other plasma environments. The experimental I–V curves in Figs. 4 and 5 obtained for inductive and capacitive methods at different plasma densities exhibit trends consistent with those predicted by OML theory. Higher plasma densities correspond to increased peak currents as the applied bias becomes more negative. The deviation from the OML-predicted I–V characteristics may result from the formation

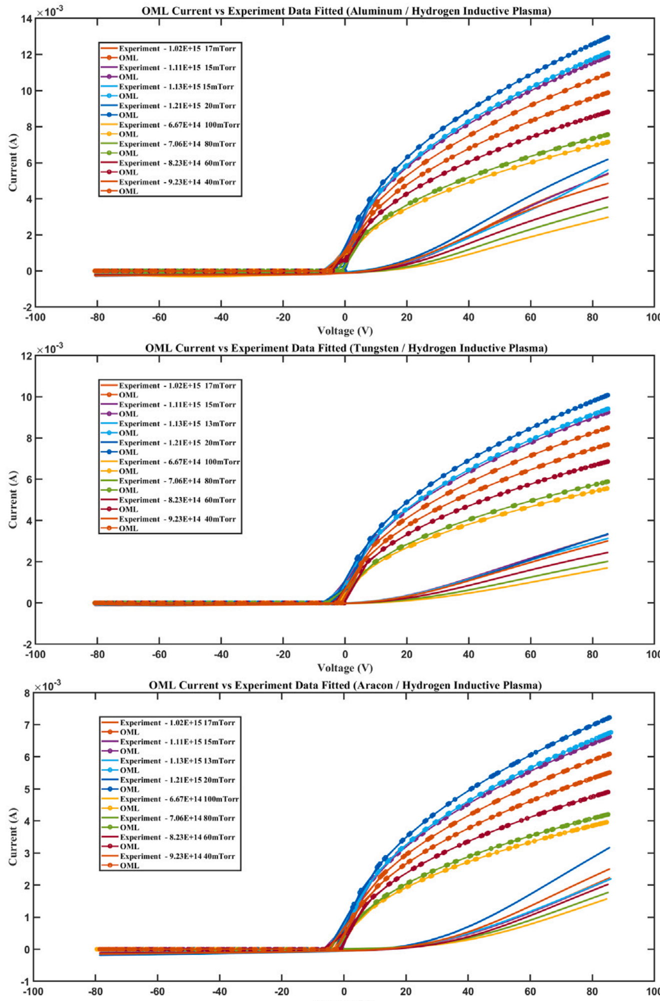

Fig. 4. Comparison of experimental hydrogen plasma densities [Table 2], Inductive plasma generation with calculated OML values.

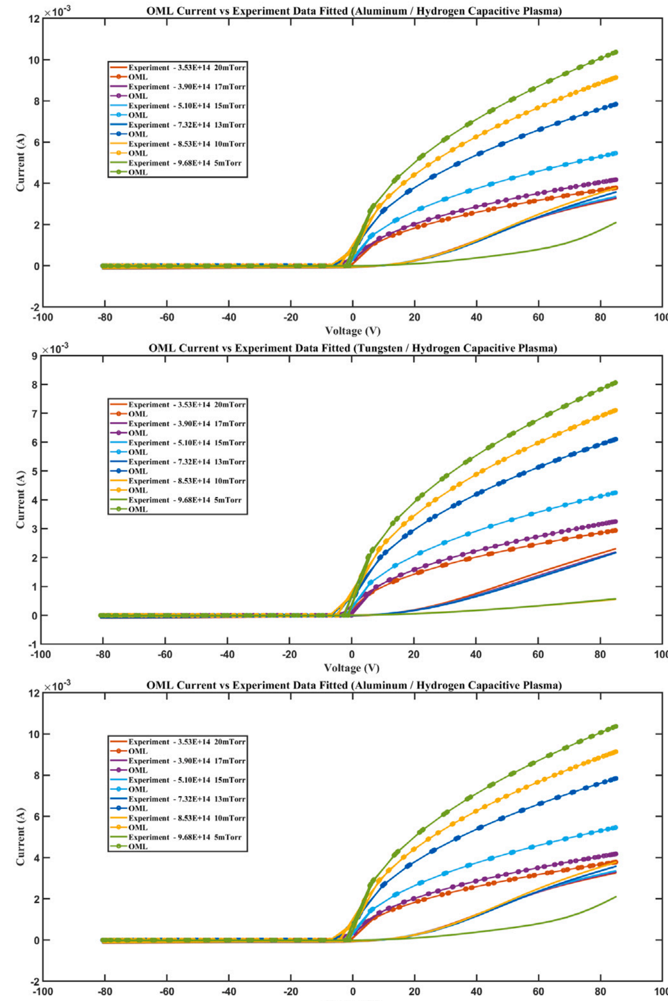

Fig. 5. Comparison of experimental hydrogen plasma densities [Table 2], Capacitive plasma generation with calculated OML values.

of secondary plasma near the probe. The presence of the secondary plasma, along with probe end effects within the chamber, result in lower current collection.

The generation of secondary plasma depends on the chamber pressure, with higher pressure resulting in increased neutral particle density available for ionization, which contributes to higher peak currents in lower densities. Higher plasma densities provide more charge carriers, thereby increasing the collected current, while elevated pressures reduce the mean free path of charged particles, increasing collisions and limiting current collection. The presence of secondary plasma formation leads to a breakdown of the OML assumptions of collisionless plasma and quasi-neutrality near the probe sheath, causing the experimental I–V curves to deviate from the ideal OML predictions. Especially at higher voltages, where the secondary electron emission can become significant, affecting the current but not accounted for in the basic OML theory. The deviations between experimental data and OML theory I-V curves at higher negative bias suggest that the OML theory may not fully capture complex plasma phenomena such as sheath dynamics, secondary electron emission, and ionization effects, especially under different material-specific conditions.

The I-V curves for tungsten, aracon, and aluminum each display unique characteristics under varying plasma densities and chamber pressures. All three materials show a similar trend where the current increases with voltage, as expected in OML predicted I-V curves. The specific peak current conditions vary slightly for each material, suggesting that surface properties and plasma-surface interactions play a role. Aracon shows a better fit between experimental and OML theory compared to tungsten and aluminum. The aluminum sample has distinct I-V curve characteristics, with the experimental ranges overlapping at higher densities. The secondary plasma generated as can be visually seen as a glow around the each sample. This behavior is observed more in capacitive plasma which could be due to the lower chamber pressure, and higher neutral particle density [10]. In the negatively biased tether, the ion current is slightly higher in oxygen and air plasma, but its magnitude is negligible compared to the electron current, resulting in I–V profiles indistinguishable across plasma conditions.

5.2. Oxygen plasma

In low Earth orbit (LEO) altitudes, O^+ ions are the dominant species. Atomic oxygen can cause degradation of the conducting materials and is a real concern for spacecraft operating in LEO. Therefore, it is crucial to investigate the influence of oxygen plasma on the electrical current generated in electrodynamic tethers. Previous experiments have used argon as the closest alternative to simulate the LEO environment, as argon is an inert gas and easy to use in a laboratory setting [8,13,14]. However, it is significantly heavier than atomic oxygen. In this experiment, we generated an oxygen plasma with densities ranging from

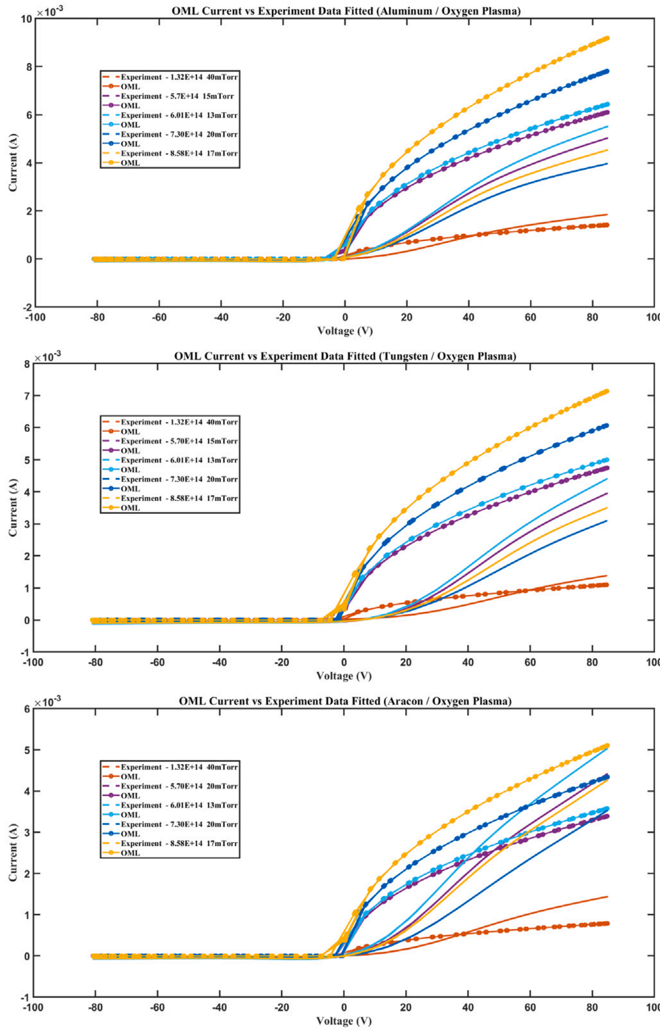

Fig. 6. Comparison of experimental oxygen plasma densities [Table 3] with calculated OML values.

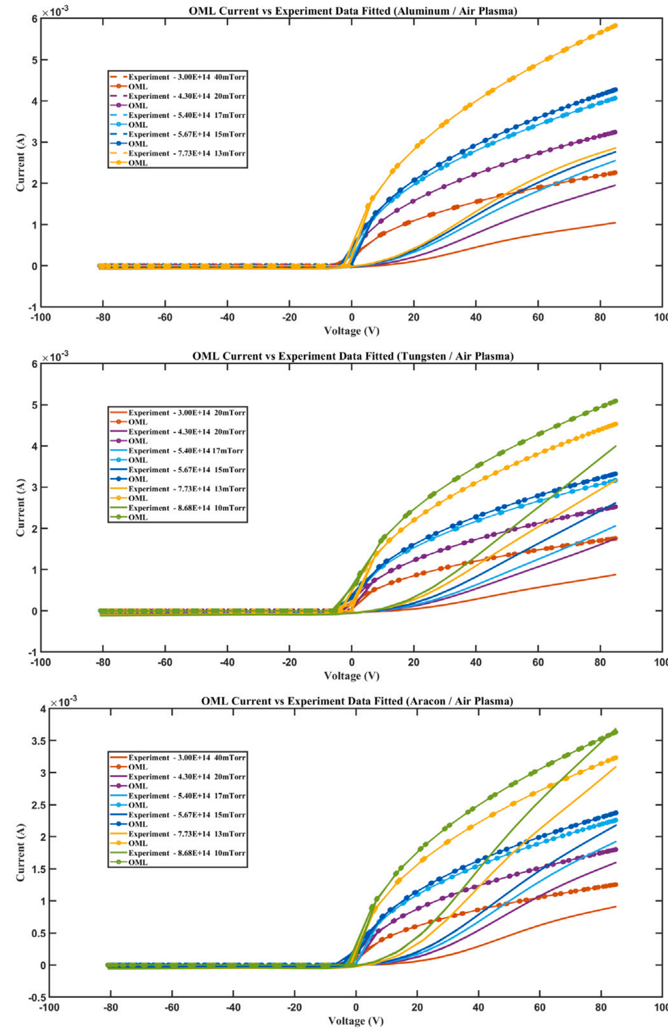

Fig. 7. Comparison of experimental air plasma densities [Table 4] with calculated OML values.

1.32×10^{14} to 8.58×10^{14} particles m^{-3} and electron temperatures between 3.3 eV and 3.6 eV. The oxygen plasma was generated exclusively using the inductive method, as stable plasma formation could not be achieved at very low or very high chamber pressures. As a result, the achievable plasma densities in the oxygen environment were lower than those obtained in hydrogen plasma.

The I-V curves generated in the oxygen plasma differ significantly from those of the hydrogen plasma. For oxygen plasma the I–V curves for oxygen plasma in Fig. 6 align with OML theoretical predictions especially at higher positive probe biases compared to hydrogen. This behavior may be attributed to differences in the ionization processes between the two gases. Additionally, the oxygen plasma data reveal anomalous trends in current scaling with plasma density. In some cases, lower-density oxygen plasmas produce I-V curves with higher current magnitudes than those observed at higher densities, an outcome that contradicts the expected OML behavior, where current typically increases with plasma density. For example, I-V curve for chamber pressure 13mTorr with density 6.01×10^{14} particles m^{-3} generates higher magnitude I-V curves in all samples than 17mTorr with density 8.58×10^{14} particles m^{-3}. These anomalies may be the result of higher neutral particle ionization. Sparks along the tether samples and glow around the sample could be seen at 80 V.

The deviation from the ideal OML values in oxygen and hydrogen plasma show how the dominant plasma ion impacts the current collection efficiency. The impact of secondary plasma generation and neutral particle collisions which are not considered in OML model is evident. These results also provide critical insights into how material selection and plasma conditions affect current collection capabilities, which is fundamental to electrodynamic tether performance in space applications. The analysis reveals distinctive current–voltage characteristics across all materials, with performance varying significantly based on plasma density and material properties. The experimental data approach the calculated OML values for the higher probe bias in oxygen plasma, especially for Aracon sample. For aluminum and tungsten samples, the variation between the experimental data and the predicted OML values is wider. The differences between experimental and theoretical values may be attributed to the unique surface properties of Aracon, which could affect the electron sheath formation around the tether. Additionally, the data indicates that the Aracon tether might collect higher currents than other samples under specific operational conditions, as suggested by previous research.

5.3. Air plasma

The air plasma was generated by ionizing the room air in the plasma chamber. Thus, the composition of the air plasma will comprise of nitrogen (78%), oxygen (20.95%), argon (0.93%), CO_2 (0.04%), and other gases in trace amounts. Utilizing air plasma is advantageous

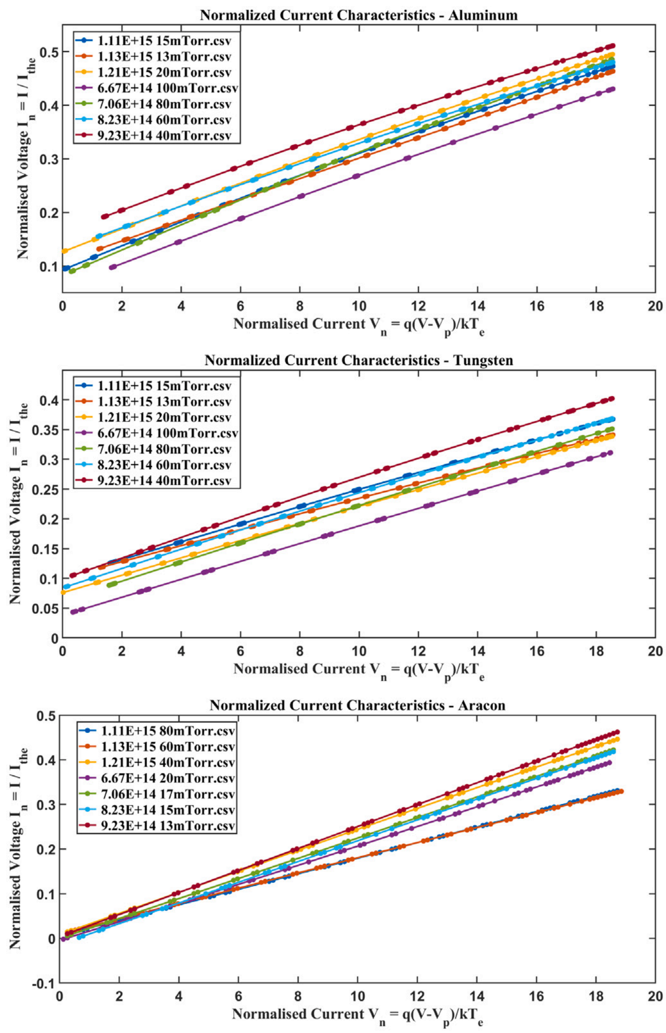

Fig. 8. Normalized voltage current curve for hydrogen inductive plasma.

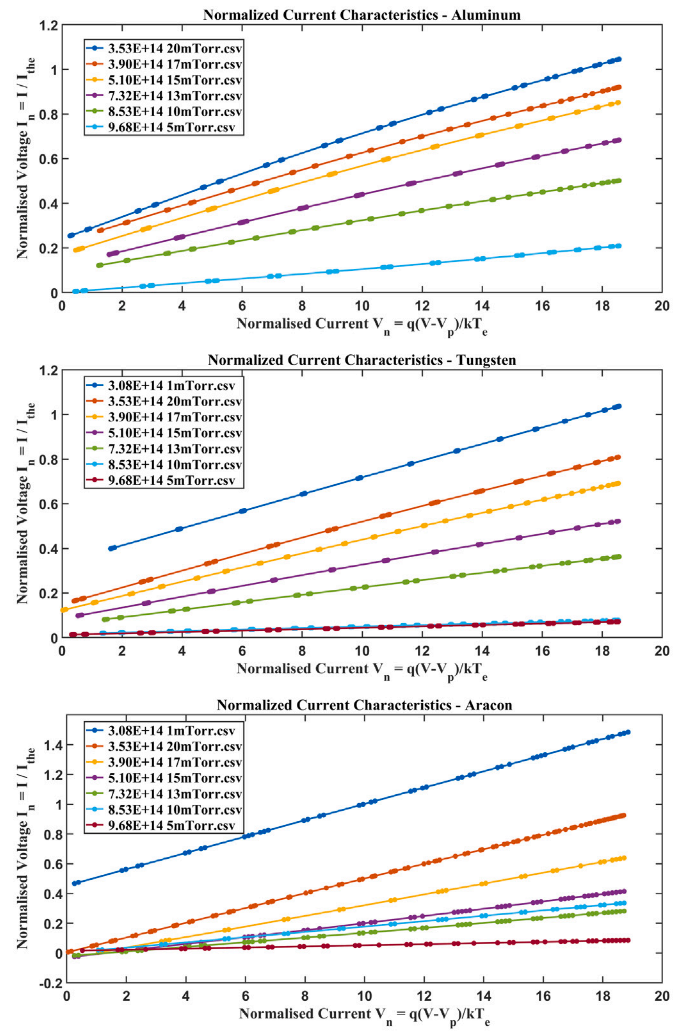

Fig. 9. Normalized voltage current curve for hydrogen capacitive plasma.

for simulating near-Earth space environments, as nitrogen is the most abundant neutral species in the lower thermosphere and ionosphere after atomic oxygen. Thus, making the experimental conditions relevant for studies of EDT performance in very low Earth orbit (VLEO). This multi-species plasma creates a more complex environment than single-gas plasmas like pure hydrogen or oxygen. The ionization energy of air plasma, composed primarily of nitrogen and oxygen, lies between the ionization energies of its two main components but is closer to nitrogen due to its dominance. The presence of heavier ions (particularly N_2^+, O_2^+, and O^+) in air plasma significantly affects the plasma dynamics and current collection properties. Since, air plasma requires more energy to ionize than pure oxygen or hydrogen plasmas.

The plasma densities generated for air plasma is from the range 3×10^{14} to 8.68×10^{14} particles m^{-3} and the plasma temperature is in the range 3.2 eV to 3.7 eV for different plasma pressures in the chamber. Fig. 7 showcases the I-V plots for each tether sample, the data is plotted across all densities simulated. The air plasma I-V curves deviate from the OML predicted values like hydrogen and oxygen. The deviation between the air plasma and the OML curves is higher than oxygen plasma I-V curves but lower than that of hydrogen plasma. The trend is likely due to the different ionization of the multi-species plasma closer to the oxygen plasma. Though a secondary plasma generation with a glow around the samples, anomalous current curves are observed in the data. The trend in the tether material is similar to that of oxygen plasma. The variation with the OML prediction is wider for the aluminum sample than for the aracon and tungsten samples.

6. Normalized current

To further analyze the I-V characteristics for each experimental scope, the data is presented in a normalized form. A Langmuir probe was used to determine the plasma potential, electron density, and electron temperature needed for normalized I-V characteristics. For the following plots, we are interested in collecting current in the electron saturation regime, thus only voltages above plasma potential are plotted ($V_p > 0$). The normalized current (I_n) is $\frac{I}{I_{the}}$, where I is the experiment current collected and the thermal current (I_{the}) is used instead of the full OML model (Eq. (1)). The voltage dependent term $\phi_p = V - V_p \ll kT_e/e$ (weak sheath effects), the OML model is simplified to thermal current (I_{the}). The normalized voltage (V_n) is calculated as $\frac{q(V-V_p)}{kT_e}$. Here $\frac{kT_e}{q}$ is the plasma's thermal energy, enabling comparison across different plasma conditions, and V_p is the measured plasma potential where the current transitions to saturation. The normalized I-V curves provide the assessment of how well the collected current follows the OML theory across different bias voltages.

The normalized I-V curves for the experimental data are plotted in the Figs. 8, 9, 10, 11. The linearity of the normalized I-V curves for the three probe materials (tungsten, aracon, and aluminum) indicates consistent electron collection mechanism that follows the general trend predicted by OML theory. However, normalized current values demonstrate a significant deviation from ideal OML prediction such as $I_n \neq 1$. The Aracon tether sample exhibits the highest normalized current

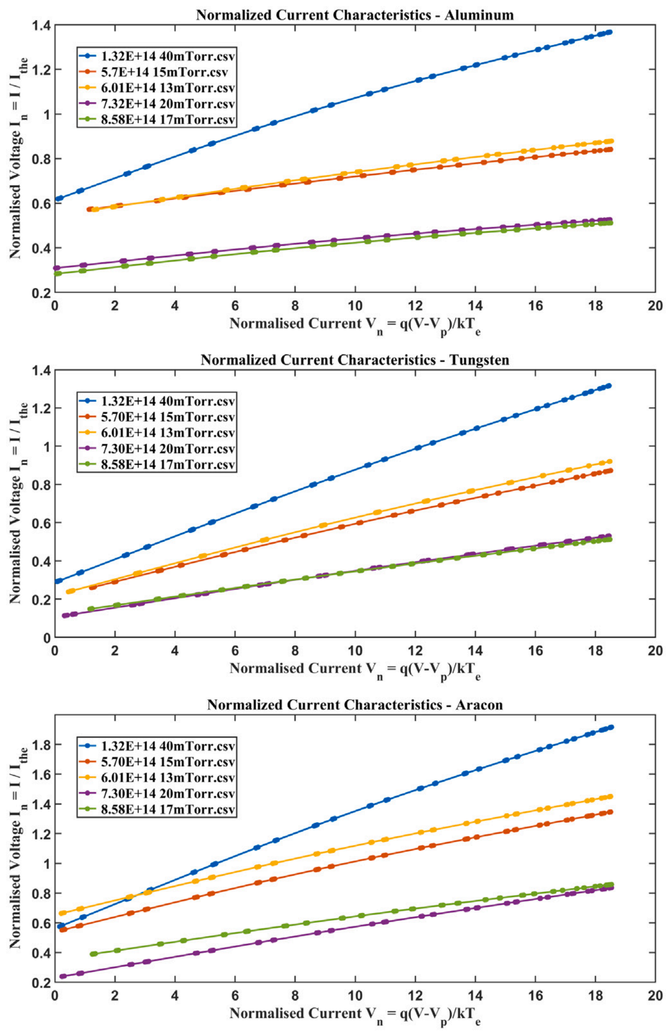

Fig. 10. Normalized voltage current curve for oxygen plasma.

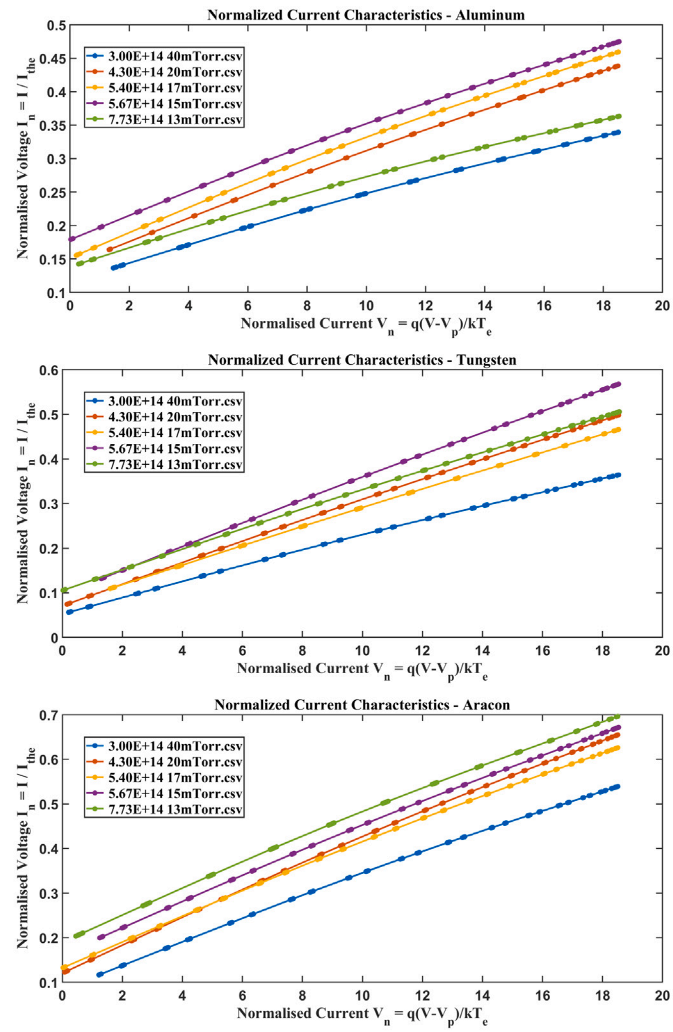

Fig. 11. Normalized voltage current curve for air plasma.

collection efficiency in oxygen and air plasma, indicating that it exceeds OML predictions more than other materials in the generated plasma conditions. However, in a hydrogen plasma, aluminum shows a higher normalized current collection comparable to that of Aracon.

For hydrogen inductive I-V curves, aluminum shows higher current near unity. Lower pressure consistently produced steeper slopes and higher pressure shows flatter curves indicating reduced collection efficiency. For hydrogen capacitive I-V curves, aracon shows highest normalized current with $I_n > 1$ for chamber pressure 1mTorr. The enhanced current collection can be attributed to secondary plasma increasing current collected. As the electron density increases with chamber pressure current collection efficiency decreases significantly across all materials likely due to particle collision effects. In oxygen plasma higher density experiment runs with $I_n < 1$ indicate reduced collection efficiency as compared to OML theory. But for density 1.32×10^{14} particles cm^{-3} oxygen I-V curves with $I_n > 1$ demonstrate enhanced current collection. With an increase in chamber pressure, the current collection efficiency decreases due to increase in particle collision with increase in density. For air plasma normalized current (I_n) values are the lowest among the three materials, with a maximum around 0.5. The increase in I_n with decreasing pressure (increasing density) indicates a significant deviation from the ideal OML behavior, likely due to collisional or probe end effects. None of the probes reach $I_n = 1$, indicating electron collection is limited by factors such as collisions, secondary plasma, sheath effects, or probe surface effects.

7. I^2 vs voltage

In this section, the electron and ion collection behavior is analyzed through the I^2 vs V plot. This method provides insights into the deviation from the OML current collection model. The I^2 vs V plot should exhibit a linear trend, non-linearity indicates the presence of sheath expansion, secondary electron emission (SEE), or space-charge limitations [15]. This analysis is important for assessing the performance of different tether material (e.g., aluminum, tungsten, and aracon for DragEN tether) and plasma species (oxygen, hydrogen, and air) in our experiments.

Figs. 12, 13, 14, 15 show the I^2 vs Voltage (V) for plasma simulated and each tether material considered. The I^2 vs Voltage (V) graph in Oxygen and Air plasma tends to approach linearity at increased applied bias and plasma density. I-V curves for hydrogen plasmas exhibit a deviation from the linear trend, particularly at lower applied biases. Oxygen plasma enables the highest current collection efficiency as a general trend for all tether material tested. The deviation from the linear trend can be attributed to the impact of ion species mass, electron temperature variations, and secondary plasma interactions on tether current collection.

The non-conducting fibers prevent secondary plasma generation which reduces the current collected leading in deviation from the OML peak currents. Thus aracon has higher alignment with OML with the experiment values approaching OML values at higher applied bias.

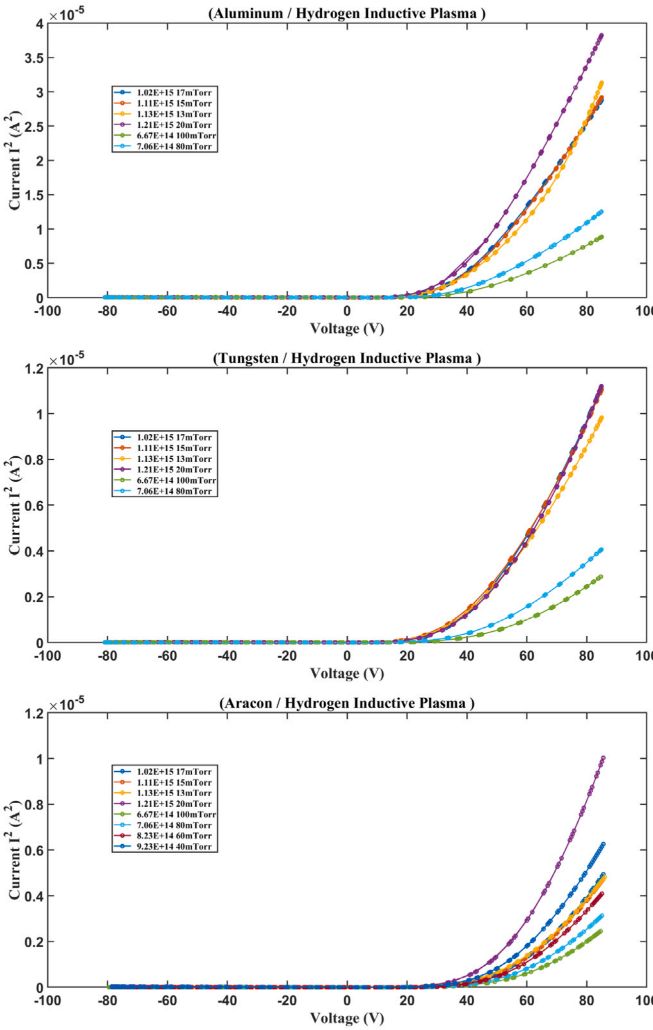

Fig. 12. I^2 vs Voltage (V) for hydrogen plasma generated with the inductive method.

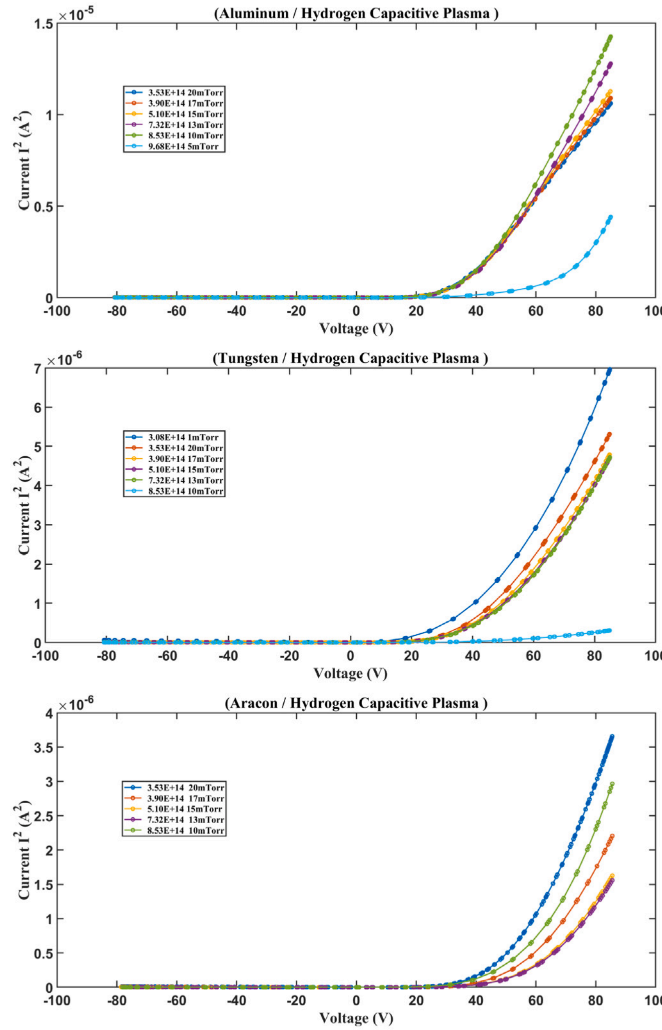

Fig. 13. I^2 vs Voltage (V) for hydrogen plasma generated with the capacitive method.

Aluminum outperforms other samples in hydrogen plasma. This would be especially beneficial since the H^+ is the dominant ion species at higher altitudes beyond 1000 km in LEO. While aracon is the obvious choice in oxygen rich environment at lower altitudes.

8. Effect of neutral gas particles

In this section, the impact of neutral particle density for the different chamber pressure in each plasma is examined. For each experiment, the operating pressure determines the neutral particle density in the plasma chamber, since the gas is weakly ionized. With the different chamber pressure used, the neutral particle density decreases with a decrease in chamber pressure. Thus, in this experiment the impact of the neutral particle density is examined for a wide range of operating pressure considered. The OML model considers a collision-less plasma thus, the impact of neutral - electron collision is often ignored. Electron–neutral collisions cause a decrease in the current collected by the tether, resulting in deviations from the OML predictions.

As discussed in previous sections two methods were used for the hydrogen plasma generation. The operating pressure in the chamber is reduced from 100mTorr to 5mTorr. This pressure variation enables testing across 20 times density range, generating a robust dataset to analyze neutral-density-dependent effects. A purple glow plasma glow is generated when the hydrogen gas is ionized in the chamber. When the tether is positively biased a faint glow along the tether can be seen, and at higher tether biasing sparks were also observed on all tether samples as seen in Fig. 16. In the capacitive method, the chamber pressure is low enough for the impact of neutral particle density on current collection to be clearly seen.

Fig. 5 indicate the anomalous current generation with the increase in neutral particle density as the chamber pressure increases. This causes deviation from OML predicted I-V curves with lower plasma densities exhibiting higher current collected. The trend can be observed in all the tether samples tested. Neutral gas released near a positively charged tether can become ionized, creating additional plasma density in the vicinity. This ionization process increases the available charged particles (particularly electrons) that can be collected by the tether [10]. Inductive plasma Fig. 4 however, do not exhibit any anomalous I-V curves. This distinct behavior indicates how plasma generation methods dictate sensitivity to neutral interactions. Additional experimental investigations would be necessary to fully characterize these effects.

When oxygen plasma is generated, a visible white hue is observed. Similar to the hydrogen plasma, at higher tether bias sparks and glow around the sample can be seen. In oxygen, instead of an uniform glow localized plasma bubbles could be seen as shown in Fig. 17. At

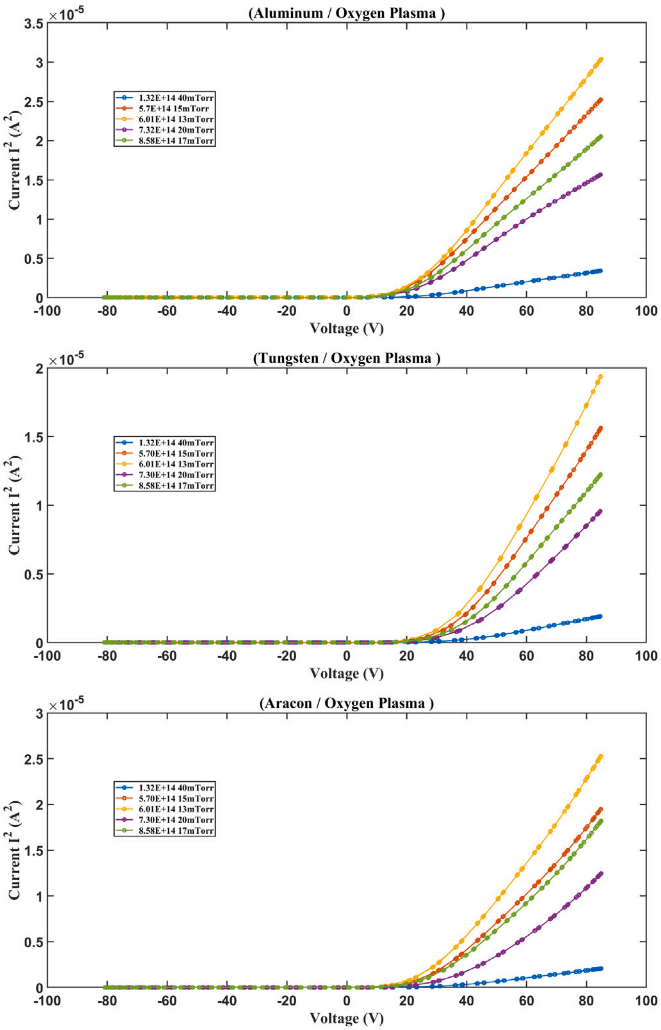

Fig. 14. I^2 vs Voltage (V) for oxygen plasma generated.

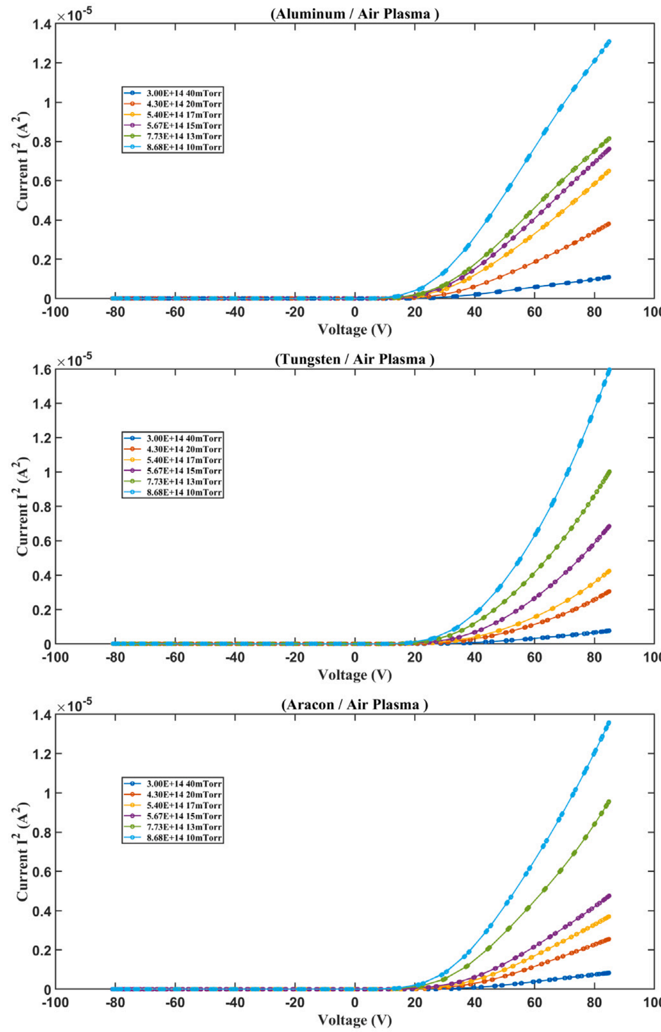

Fig. 15. I^2 vs Voltage (V) for air plasma generated.

the lower operating pressure, faint pulsations of plasma were detected with sparking along the tether sample lengths. Aracon sample shows the highest sparking and glow. The aluminum and tungsten sample experiment runs had faint sparks and glow around the sample. The observed variation in density-dependent I-V curve trends between oxygen plasma and air plasma is not uniform. From Fig. 6, It was seen that the experiment run with the density 6×10^{14} particles m^{-3} had higher I-V curve than the largest density simulated. In fact, the scope I-V curves for the 6×10^{14} particles m^{-3} and 5.7×10^{14} particles m^{-3} have higher I-V curves than the 8.5×10^{14} particles m^{-3}. The anomalous current generated in oxygen plasma further indicates how the presence of neutral particle density can increase the current collected in a tether.

The orange-pink hue of air Plasma can be seen in Fig. 18. Similar to the oxygen plasma experiment runs, plasma bubbles could be seen at high positive tether biasing. When the bias is applied a uniform glow os secondary plasma around the samples can be seen. Even a slight pulsating secondary plasma can be seen at higher applied bias. When examining a tungsten sample, plasma bubbles instead of a uniform glow was observed. Unlike hydrogen and oxygen plasma, no anomalous current in the experiment runs was observed in Fig. 7.

In previous experiment, impact of neutral particle density was observed at low vacuum (higher chamber pressures) [10]. In this experiment, similar phenomenon was observed apart in hydrogen and oxygen plasma. The air plasma did not exhibit anomalous current in I-V

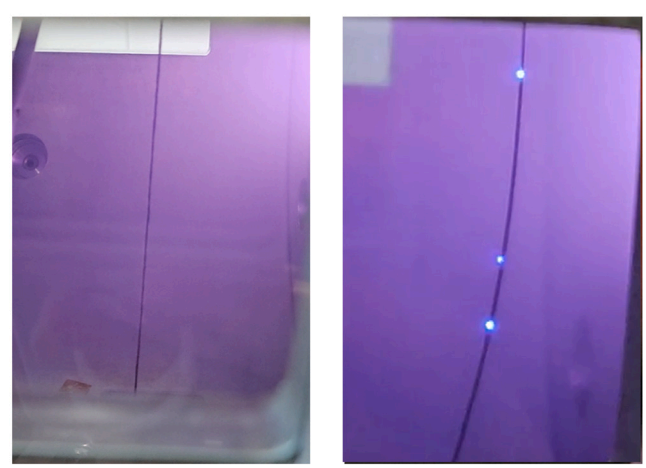

Fig. 16. Secondary plasma and sparks due to secondary plasma generation induced in hydrogen plasma.

curves. In hydrogen plasma, the anomalous current was more prevalent in capacitive I-V profiles. Lower pressures in capacitive profiles

Fig. 17. Secondary plasma and sparks due to secondary plasma generation induced in oxygen plasma.

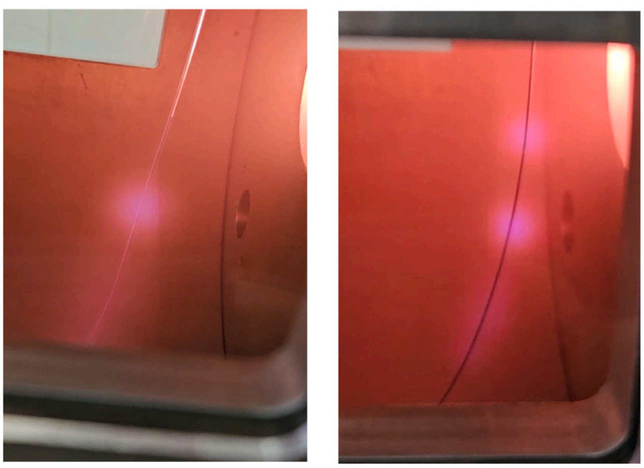

Fig. 18. Secondary plasma generation around the tether sample in form of plasma bubbles induced in air plasma.

reduce neutral density, minimizing collisions and aligning results with collisionless OML assumptions, yielding higher measured currents.

9. Conclusion

This study investigated the impact of different ion species using different tether material on the electron current collection efficiency of EDTs under laboratory generated plasma conditions representative of low Earth orbit (LEO). Experiments were conducted using hydrogen, oxygen, and air plasmas with various densities and chamber pressures using aluminum, tungsten and aracon as tether samples. The results showed the impact of plasma composition and tether material on current collection. The Aracon sample demonstrated superior current collection efficiency in oxygen and air plasmas, while aluminum performed better in hydrogen plasma environments. Tungsten exhibited lower current collection across most conditions. Significant deviations from OML theory were observed, especially at higher plasma densities is observed due to the presence of secondary plasma formation and neutral particle effects. The experiments highlighted the influence of neutral particle density and secondary plasma generation on current collection, factors not accounted for in the simplified OML model. Sparks, plasma bubbles, and secondary plasma glow around the tether samples further emphasize the complex plasma-tether interactions that occur in realistic environments. The normalized current analyses confirmed that none of the tether samples fully achieved the ideal OML current collection, indicating limitations due to collisions, sheath dynamics, and material surface effects. These findings highlight the importance of selecting appropriate materials and understanding environmental plasma conditions when designing EDT systems for propulsion and power generation applications in LEO and VLEO.

CRediT authorship contribution statement

Shagun Aggarwal: Writing – review & editing, Writing – original draft, Project administration, Methodology, Investigation. **Josef Richmond:** Data curation, Resources. **Andrew Dempster:** Supervision. **Jason Held:** Supervision. **Rod Boswell:** Supervision.

Declaration of competing interest

The authors declare that they have no known competing financial interests or personal relationships that could have appeared to influence the work reported in this paper.

References

[1] M. Dobrowolny, N.H. Stone, A technical overview of TSS-1: the first tethered-satellite system mission, Il Nuovo Cimento C 17 (1994) 1–12.
[2] N.H. Stone, C. Bonifazi, The TSS-1R mission: Overview and scientific context, Geophys. Res. Lett. 25 (4) (1998) 409–412.
[3] Mario D. Grossi, Plasma Motor Generator (PMG) Electrodynamic Tether Experiment, Technical report, 1995.
[4] Les Johnson, Brian Gilchrist, Enrico Lorenzini, Nobie Stone, Ken Wright, Propulsive small expendable deployer system (proseds) experiment: Mission overview & status, in: 39th AIAA/ASME/SAE/ASEE Joint Propulsion Conference and Exhibit, 2003, p. 5094.
[5] J.R. Sanmartin, Manuel Martínez-Sánchez, E. Ahedo, Bare wire anodes for electrodynamic tethers, J. Propuls. Power 9 (3) (1993) 353–360.
[6] Space Plasma Power and Propulsion Group, URL https://physics.anu.edu.au/research/npaa/sp3.
[7] Brian E. Gilchrist, Sven G. Bilén, Éric Choinière, Alec D. Gallimore, Timothy B. Smith, Analysis of chamber simulations of long collecting probes in high-speed dense plasmas, IEEE Trans. Plasma Sci. 30 (5) (2002) 2023–2034.
[8] Jean-Michel Siguier, Pierre Sarrailh, Jean-François Roussel, Virginie Inguimbert, Gael Murat, Juan SanMartin, Drifting plasma collection by a positive biased tether wire in LEO-like plasma conditions: current measurement and plasma diagnostic, IEEE Trans. Plasma Sci. 41 (12) (2013) 3380–3386.
[9] Keith Fuhrhop, Eric Choiniere, Brian Gilchrist, A comparison of laboratory experimental and theoretical results for electrodynamic tether electron collection performance for some bare tether geometries, in: AIAA SPACE 2009 Conference & Exposition, 2009, p. 6659.
[10] Koki Kashihara, Mengu Cho, Satomi Kawamoto, Ground experiments and computer simulations of interaction between bare tether and plasma, IEEE Trans. Plasma Sci. 36 (5) (2008) 2324–2335.
[11] Avish Gupta, Varun Thakurta, Dhananjay Sahoo, Anirudh Kailaje, Design and analysis of a passive tether de-orbiting mechanism for a nano-satellite, in: 2019 IEEE Aerospace Conference, IEEE, 2019, pp. 1–10.
[12] Pascal Chabert, Tsanko Vaskov Tsankov, Uwe Czarnetzki, Foundations of capacitive and inductive radio-frequency discharges, Plasma Sources Sci. Technol. 30 (2) (2021) 024001.
[13] Jesse McTernan, Sven Bilen, Iverson Bell, Brian Gilchrist, Current collection to and plasma interaction with femtosatellite-and CubeSat-scale electrodynamic tether subsystems, in: AIAA SPACE 2012 Conference & Exposition, 2012, p. 5295.
[14] Masaya Kozakai, Haruki Takegahara, Evaluation of plasma contactor ground experiments for electrodynamic tether, 2001, pp. 01–242, IEPC Paper.
[15] Francis F. Chen, Langmuir probe diagnostics, in: IEEE-ICOPS Meeting, Jeju, Korea, vol. 2, (6) Citeseer, 2003.